

UDC 539.171

<sup>1</sup>Burtebayev N., <sup>1,2\*</sup> Alimov D.K., <sup>3</sup>Boztosun I., <sup>1</sup>Kerimkulov Z., <sup>1</sup>Nassurlla M.,  
<sup>1,2</sup>Mukhamejanov Y.S., <sup>2</sup>Yushkov A.V., <sup>1</sup>Sakhiev S.K., <sup>4</sup>Janseitov D.M.,  
<sup>5</sup>Bahtibayev A.N., <sup>5</sup>Pattaev A. and <sup>6</sup>Hamada Sh.

<sup>1</sup>Institute of Nuclear Physics, Almaty, Kazakhstan

<sup>2</sup>Department of Physics and Technology, al-Faraby KazNU, Almaty, Kazakhstan

<sup>3</sup>Faculty of Science Department of Physics, Akdeniz University, Antalya, Turkey

<sup>4</sup>Physics and Technology Department, Eurasian National University, Astana, Kazakhstan

<sup>5</sup>Natural Sciences Faculty, A. Yesevi IKTU, Turkestan, Kazakhstan

<sup>6</sup>Faculty of Science, Tanta University, Tanta, Egypt

\*e-mail: Diliyo@mail.ru

## Investigation of interaction processes of $^3\text{He}$ with $^{14}\text{N}$ nuclei at 50 and 60 mev

**Abstract:** Elastic scattering of  $^3\text{He}$  on  $^{14}\text{N}$  as example of 1p-shell nuclei at 50 and 60 MeV has been investigated within the framework of Optical Model. In the Optical Model analysis, both microscopic double-folding and phenomenological potentials for the real part of the complex nuclear potential have been used. For both microscopic double-folding and phenomenological analysis, the imaginary potential has taken to be Wood-Saxon volume shaped. It is noticed that while a normalization of the strength of the double-folding real potential is needed to explain the structure observed in the experimental data, a good agreement between experimental data is obtained for the phenomenological potential case.

**Key words:** optical model, double-folding potential, elastic and inelastic scattering, nucleon-nucleon interaction, fresco.

### Introduction

The study of the interaction of  $^3\text{He}$  with  $^{14}\text{N}$  nuclei at low energies is of interest both from the point of view of establishing reliable values of the parameters of the internuclear interaction potential of  $^3\text{He}$  and to study the mechanisms of cluster effect in scattering processes [1].

The elastic and inelastic experimental data of  $^3\text{He}+^{14}\text{N}$  system has been measured in Institute of Nuclear Physics (INP), Almaty as a part of larger experimental research program of the scattering of  $^3\text{He}$  on light-heavy nuclei with a mass range between 4 and 28. Experiment on the elastic and inelastic scattering of  $^3\text{He}$  ions with energies 50 and 60 MeV on  $^{14}\text{N}$  were carried out on the extracted beam of the isochronous cyclotron U-150M in INP Almaty, Kazakhstan. The spread of the beam energy was less than 1%.

### Experimental details

In order to carry out measurements on gas targets a special device [2], a cylinder filled with the studied isotope having input and output windows for

the accelerated particles beam made of iron foil ( $7\text{ mg/cm}^2$ ) on indium seals, has been developed and manufactured. Nitrogen isotope  $^{14}\text{N}$  (enrichment equal to 99.63%) target thickness was equal to  $1.37\text{--}7.66\text{ mg/cm}^2$ . For the reaction products registration there is a window with radial diameter equal to cylinder quarter diameter made of Mylar ( $2.9\text{ mg/cm}^2$ ). The exit window is arranged so that the geometrical axis of limiting collimator (having a slope relative to the horizontal plane of the scattering camera equal to  $10^\circ$ ), installed before turning spectrometer always intersects the center of the target gas. The target was mounted in the scattering chamber in two positions for measuring the angular range between  $10^\circ$  to  $96^\circ$  and from  $84^\circ$  to  $170^\circ$ ; in last case it must be rotated around a vertical axis  $180^\circ$ . Calculations of the thickness of the target was carried out using vacuum-gauge according to the formula:

$$d = \rho Pt, \quad (1)$$

where  $\rho$  – density of the gas under normal conditions,  $P$  – pressure,  $t$  – the visible part of the beam seen by collimator, defined as:

$$t = \left( R - d_1 l / (d_1 + d_2) \right) \sin \alpha \left( 1 / \sin(\theta + \alpha) + 1 / \sin(\theta - \alpha) \right) (2), \quad (2)$$

where  $d_1$  and  $d_2$  – collimator diaphragms,  $R$  – the distance from the center of the gas target to the current diaphragm  $d_1$ ,  $l$  – distance between the diaphragms,  $\alpha$  – angular uncertainty which, as shown in Figure 1, is calculated from the relationship:

$$\tan \alpha = d_2 / 2l \quad (3)$$

### The geometry of the cross-section of the target gas in the reaction plane

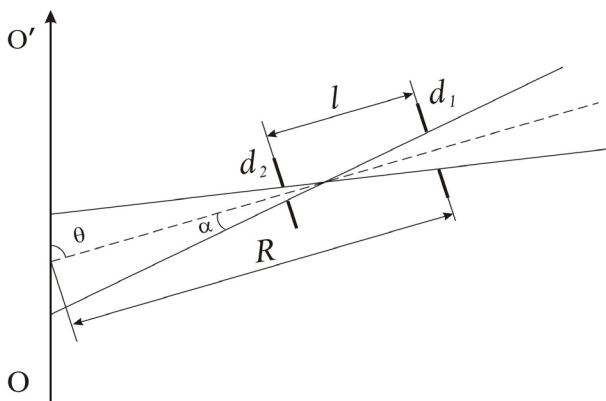


**Figure 1** –  $O'O$  – direction of the ion beam,  $d_1$  and  $d_2$  – limiting collimator diaphragms,  $\alpha$ - angular uncertainty,  $\theta$  – scattering angle,  $R$  – the distance from the center of the target to the operating diaphragm ( $d_1$ ) spectrometer,  $l$  – distance between the diaphragms

The value of the calculated thickness of the gas defined this way column is underestimated by up to 3% of the real at angle of  $90^\circ$  and 1-2% at angle  $170^\circ$  in the laboratory coordinate system (lcs). This decrease is due to both the deviation of the gas from the cylindrical cord due to the divergence of the beam after forming input collimator and the limited visibility of the cord conical solid angle of the detector, instead of flat sections that were used in the calculations.

The thickness of the gas target was determined by weighing or by energy loss of  $\alpha$  - particles from a radioactive source with exactly 6-9%. Nuclear reaction products were detected by using telescope detectors consisting of surface-barrier silicon counters with a thickness - 10, 18, 33, 50, 100 micrometers or ionization chamber, the effective

thickness may be smoothly changed in a broad range. In both variants, telescopes as E-counter used diffusion-drift silicon detectors with a sensitive layer thickness of 2 mm. The angular distributions of scattered particles in the investigated nuclei were measured in the angular range of  $10^\circ$ - $170^\circ$  in laboratory coordinate system in steps  $3^\circ$  [3].

Experimental data  $^3\text{He}+^{14}\text{N}$  measured at INP Almaty has been analyzed within the standard optical model and microscopic double-folding potentials using the computer code FRESKO. In the next section we present our optical model potentials and then show our results in section 4. We also present our conclusion and future plots in this section.

### The Model

In the present calculations, we have used both phenomenological deep and double-folding real potentials with a volume type imaginary potential [4-8]. Our total real potential for these cases consists of the nuclear potential,  $V_{Nuclear}$  and the Coulomb and centrifugal potentials,  $V_{Coulomb}$ ,  $V_{Centrifugal}$  respectively.

$$V_{total} = V_{Nuclear}(r) + V_{Coulomb}(r) + V_{Centrifugal}(r). \quad (4)$$

The phenomenological nuclear potential is assumed to have the square of a Woods-Saxon shape.

$$V_{Nuclear}(r) = \frac{-V_0}{\left(1 + \exp(r - R)/a\right)^2}, \quad (5)$$

where

$$R = r_0 \left( A_p^{1/3} + A_t^{1/3} \right) \quad (6)$$

The Coulomb potential [5] due to a charge  $Z_p e$  interacting with a charge  $Z_t e$  distributed uniformly over a sphere of radius  $R_C$ , is also added.

$$V_{Coulomb} = \frac{1}{4\pi\epsilon_0} \frac{Z_p Z_t e^2}{r}, \quad r \geq R_C, \quad (7)$$

$$\frac{1}{4\pi\epsilon_0} \frac{Z_p Z_t e^2}{2R_C} \left( 3 - \frac{r^2}{R_C^2} \right), r < R_C, \quad (8)$$

where  $R_C = 4.62$  fm is the Coulomb radius, and  $Z_p$  and  $Z_t$  denote the charges of the projectile  $p$  and the target nuclei  $t$  respectively.

**Table 1** – Optical and Double-Folding potential parameters with normalization coefficient  $N_r$

$E_b(\text{MeV})$	$V_0(\text{MeV})$	$r_0(\text{fm})$	$a_0(\text{fm})$	$W_V(\text{MeV})$	$r_V(\text{fm})$	$a_V(\text{fm})$	$N_r$	$R_C(\text{fm})$
50 DF	60	1.2	0.823	8.8 8.8	1.412 1.412	0.747 0.747	0.9	4.62
60 DF	55	1.2	0.823	9.8 9.8	1.318 1.318	0.747 0.747	0.9	4.62

Double-Folding potential [6] is calculated by using the nuclear matter distributions of both projectile and target nuclei together with an effective nucleon-nucleon interaction potential ( $v_{NN}$ ) are used. Thus, the double-folding potential is

$$V_{DF}(r) = \int dr_1 \int dr_2 \rho_p(r_1) \rho_t(r_2) v_{NN}(r_{12}), \quad (9)$$

where  $\rho_p(r_1)$  and  $\rho_t(r_2)$  are the nuclear matter density of projectile and target nuclei, respectively. Gaussian density distributions (GD) have been used for both nuclei [4, 7] defined as:

$$\rho(r) = \rho_0 \exp(-\beta r^2) \quad (10)$$

$$V_{NN}(r) = 7999 \frac{\exp(-4r)}{4r} - 2134 \frac{\exp(-2.5r)}{2.5r} + J_{00}(E) \delta(r) \text{ MeV}, \quad (12)$$

where

$$J_{00}(E) = 276 \left[ 1 - 0.005 E_{Lab} / A_p \right] \text{ MeVfm}^3. \quad (13)$$

### Results and Conclusion

The results obtained by using the microscopic double-folding and phenomenological nuclear potentials with the above-described models are shown in Fig.1 in comparison with the experimental data. As it can be seen from this figure that the real part of the double folding potential requires a

where  $\beta$  is adjusted to reproduce the experimental value for the rms radius of the  $^{14}\text{N}=2.58$  fm and  $^3\text{He}=1.877$  fm [8].  $\rho_0$  values can be obtained from the normalization condition

$$\int \rho(r) r^2 dr = \frac{A}{4\pi}, \quad (11)$$

where  $A$  is the mass number. We have chosen the most common one, the M3Y nucleon-nucleon realistic interaction. The M3Y has two form, one of them to M3Y-Reid and another is based on the so-called M3Y-Paris interaction [7]. In this work, we use the former form with the relevant exchange correction term due to the Pauli principle, given by

normalization in order to obtain a reasonable result. Without this normalization,  $N_r = 0.9$ , we could not get an agreement with the experimental data. The phenomenological Woods-Saxon typed potential has provided a better agreement with the experimental data as seen in the same figure with green line.

Double-Folding analysis could effectively fit the experimental data at the first hemisphere (angles lower than  $70^\circ$ ), while phenomenological analysis could fit the experimental data at backward angles. The resulting potentials can be used for model calculations of yields of nuclear reactions necessary for astrophysical applications.

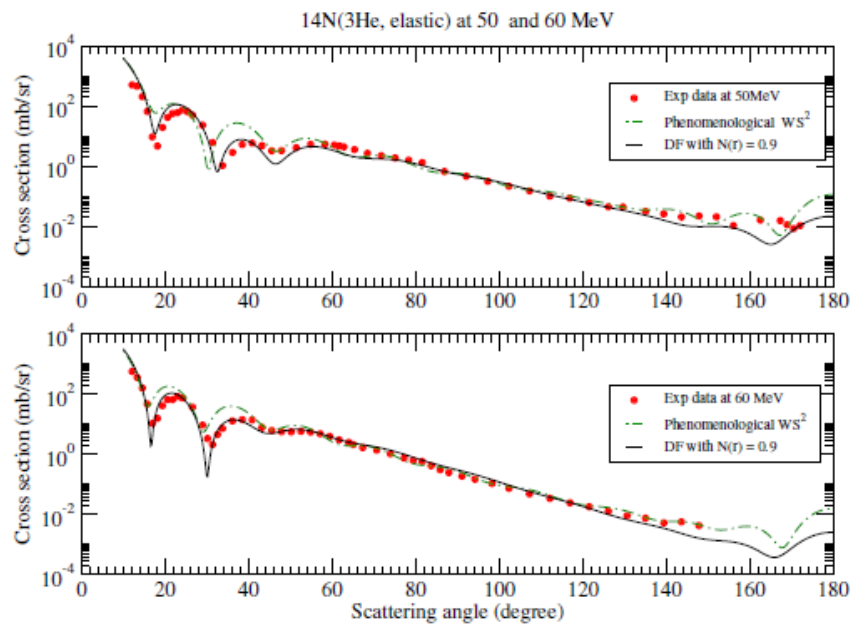


**Figure 2** – The results of Double-Folding and phenomenological Wood-Saxon squared potentials in comparison with experimental data for  $^3\text{He}+^{14}\text{N}$  system at 50 and 60 MeV

## References

1. Burtebayev N., Hamada Sh., Kerimkulov Zh., Alimov D.K. and Yushkov A.V. Clusterization probability in  $^{14}\text{N}$  nuclei // WASET. – 2014. – Vol. 86. – P. 630-634.
2. Duysebaev A.D., Ivanov G.H., Burtebayev N.T., Berger A.A., Arzumanova Z.M. Gas target // Izv. AN KazSSR. – 1984, – Vol. 4. – P. 73-74.
3. MAESTRO-32 MCA Emulator for Microsoft Windows 98. 2000. NT. and XP A65-B32 Software // Users Manual Software Version 6.
4. Burtebayev N., Alimov D.K., Boztosun I. and et.al. Interaction of  $1p$  nuclei: Case of  $^{14}\text{N}+^{12}\text{C}$  Elastic Scattering at 21.0 MeV // Journal of Physics. Conference Series. – Turkey. – 2015. – Vol. 590. – P. 1-5.
5. Kucuk Y. and Boztosun I. Global examination of the  $^{12}\text{C} + ^{12}\text{C}$  reaction data at low and intermediate energies // Nucl. Phys. A. – 2006. – Vol. 764. – P. 160-180.
6. Stock R., Jahnke U., Hendrie D. L., Mahoney J., Maguire C. F., Schneider W.F.W., Scott D. K. and Wolschin G. Contribution of alpha cluster exchange to elastic and inelastic  $^{16}\text{O}+^{20}\text{Ne}$  scattering // Phys. Rev. C. – 1976. – Vol. 14. – P. 1824 – 1831.
7. Karakoc M. and Boztosun I.  $\alpha$ - $\alpha$  double folding cluster potential description of the  $^{12}\text{C}+^{24}\text{Mg}$  system // Phys. Rev. C. – 2006. – 73. – 047601. – P. 1-4.
8. Vries H.De., Jager C.W.De. and Vries C. De. At. Data and Nucl. Data Tables. – 1987. – Vol. 36. – P. 495.